AIAA JOURNAL
Vol. 31, No. 6, June 1993

Unsteady Transonic Two-Dimensional Euler Solutions Using Finite Elements

Gary A. Davis* and Oddvar O. Bendiksen†
University of California, Los Angeles, Los Angeles, CA 90024

A finite element solution of the unsteady Euler equations is presented, and demonstrated for two-dimensional airfoil configurations oscillating in transonic flows. Computations are performed by spatially discretizing the conservation equations using the Galerkin weighted residual method and then employing a multistage Runge-Kutta scheme to march forward in time. Triangular finite elements are employed in an unstructured O-mesh computational grid surrounding the airfoil. Grid points are fixed in space at the far-field boundary and are constrained to move with the airfoil surface to form the near-field boundary. A mesh deformation scheme has been developed to efficiently move interior points in a smooth fashion as the airfoil undergoes rigid-body pitch and plunge motion. Both steady and unsteady results are presented, and a comparison is made with solutions obtained using finite volume techniques. The effects of using either a lumped or consistent mass matrix were studied and are presented. Results show the finite element method provides an accurate solution for unsteady transonic flows about isolated airfoils.

I. Introduction

THE accurate determination of the unsteady flowfield surrounding an oscillating airfoil or wing in transonic flow is of paramount importance in the prediction of the flutter characteristics of the body. Transonic flutter remains an active research topic because of the continued interest by both the military and commercial sectors to operate in these flight regimes with vehicles that are ever lighter and, as a result, more flexible. Typically, analysis of fluid-structure interaction in flight vehicles involves describing the vehicle structure using finite elements, whereas finite difference methods are used to model the surrounding fluid. Coupling of the two dissimilar models then presents problems because of the disparity between the two solution techniques. Additional complexities arise because of phase mismatching between the fluid pressures and the displacements of the structure. It seems a natural progression to use finite element methods to describe the behavior of both the fluid and structure, thus bringing more commonality into the analysis of the two media.

Early research efforts concentrated on using the transonic small-disturbance equation or the nonlinear full potential equation as the model for the gas dynamic behavior in transonic flows. Unfortunately, this idealization leads to errors when strong shocks are present because of their inability to account for the production of entropy and vorticity. To properly account for these effects within the framework of the conservation laws, the Euler equations must be used. These equations, although they neglect fluid viscosity, have become the standard when unsteady transonic solutions are desired. The absence of a viscosity representation is an important limitation of the present formulation and must be considered carefully when computing solutions. It is well known that the presence of a boundary layer can significantly alter the shock position and therefore affect the overall airfoil lift and drag. At present we restrict our work to those cases that we feel are not unduly affected by viscosity.

A variety of methods have been developed to obtain numerical solutions to the Euler equations of gas dynamics for steady flows.[1] Many of these techniques have matured to the point that accurate solutions for transonic flows about complex geometries have been obtained.[2] Of the many different schemes reported in the literature, the finite volume methods developed by Jameson et al.,[3] Jameson and Mavriplis,[4] and Mavriplis[5] have become quite popular. These schemes, while not providing shock resolution of as high a quality as upwind based methods,[6] are less expensive from a computational standpoint and therefore well suited for unsteady flow calculations.

The evolution of numerical methods for unsteady applications has lagged development of steady flow schemes by about 5 years. Edwards and Thomas[7] present a survey of the various methods that have been used for unsteady transonic flows. As with steady flows, there are a number of references that delineate finite volume techniques and their use in unsteady problems. Venkatakrishnan and Jameson[8] describe unsteady flow solutions using finite volume schemes where the flow variables are stored in the center of each cell. In a recent series of papers, Batina[9,10] has reported the use of finite volume schemes for unsteady flow calculations in which information is stored at the nodal points of the cells and linearly interpolated at points in the cell interior.

In the work at hand we present a finite element analysis of unsteady transonic flow. Our immediate objective is to demonstrate the feasibility of a computational approach consistent with the finite element method widely used in structural applications. The ultimate goal, which will be addressed in future papers, is an eventual unification of the structural and fluid equations, along the lines proposed in Ref. 11.

II. Euler Equations

In this paper, finite element solutions of the two-dimensional Euler equations are presented for steady and unsteady transonic flows. These equations, which are the basic statements of conservation of mass, momentum, and energy in the

Presented as Paper 92-2504 at the AIAA/ASME/ASCE/AHS/ASC 33rd Structures, Structural Dynamics, and Materials Conference, Dallas, TX, April 13-15, 1992; received July 9, 1992; revision received Oct. 2, 1992; accepted for publication Oct. 2, 1992.

*Graduate Student Researcher, Mechanical, Aerospace, and Nuclear Engineering Department. Member AIAA.

†Associate Professor, Mechanical, Aerospace, and Nuclear Engineering Department. Member AIAA.

absence of viscous forces, are written as follows in a mixed Lagrangian-Eulerian formulation:

$$\frac{\mathrm{d}}{\mathrm{d}t}\int_{S(t)} w\,\mathrm{d}A + \int_{S(t)}\left(\frac{\partial f}{\partial x}+\frac{\partial g}{\partial y}\right)\mathrm{d}A = 0 \tag{1}$$

where

$$w = \begin{bmatrix}\rho\\ \rho u\\ \rho v\\ \rho E\end{bmatrix}, f = \begin{bmatrix}\rho(u-U)\\ \rho u(u-U)+p\\ \rho v(u-U)\\ \rho E(u-U)+pu\end{bmatrix}, g = \begin{bmatrix}\rho(v-V)\\ \rho u(v-V)\\ \rho v(v-V)+p\\ \rho E(v-V)+pv\end{bmatrix} \tag{2}$$

In the previous equations the variables ρ, p, and E are the density, pressure, and specific total energy, respectively. The Cartesian velocity components of the fluid are given by u and v, and the mesh velocity components are U and V. Here the region of integration $S(t)$ is not required to be a material region; thus it may deform in any arbitrary manner.

The specific total energy E is defined relative to the specific internal energy e and the fluid velocity components by

$$E = e + \tfrac{1}{2}(u^2+v^2) \tag{3}$$

Finally, an equation of state is specified to relate the flow variables to the static pressure:

$$p = \rho e(\gamma - 1) \tag{4}$$

III. Spatial Discretization

To use the finite element method as a vehicle for solution of the Euler equations, the flowfield surrounding the airfoil is partitioned into a large number of small triangular elements. This element shape was chosen for the present work because it represents the simplest planar figure that can be developed from straight lines. Triangles have been used extensively in structural finite element work, and a large body of information exists concerning element interpolation and integration.

A. Galerkin Method

Here we present the discretization of the Euler equations using the well-known Galerkin weighted residual method common in structural finite elements.[12] This method, which operates on the differential form of the conservation laws, seeks to minimize error with respect to a set of weight functions.

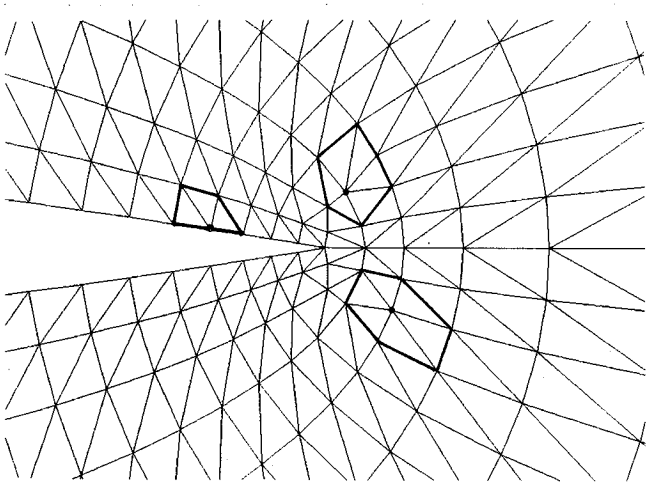

Fig. 1 Typical control volumes consisting of a collection of elements and a common node point.

Applied to the basic conservation laws, the Galerkin method can be stated as

$$\frac{\mathrm{d}}{\mathrm{d}t}\int_{S(t)} \phi_i w\,\mathrm{d}A + \int_{S(t)}\phi_i\left(\frac{\partial f}{\partial x}+\frac{\partial g}{\partial y}\right)\mathrm{d}A = 0 \tag{5}$$

where the region of integration $S(t)$ consists of a control volume associated with a node point and is taken as the collection of elements that share a common node. Figure 1 defines several typical control volumes in the trailing-edge region of the airfoil used in the present work. The weight functions ϕ_i are chosen to be piecewise linear functions that vary from unity at the node point i to zero at all other nodes in the control volume. Thus Eq. (5) represents one equation set for each node point in the mesh.

We complete the discretization by introducing an interpolation rule to obtain flow variable quantities at interior points in an element from nodal values. The interpolation is given by

$$w(x, y, t) = \sum_{j=1}^{3}\phi_j(x,y)\, w_j(t) \tag{6}$$

where $w_j(t)$ are the flow variables at the node points of the element and the linear interpolation functions ϕ_j are the same as those used in the Galerkin statement of Eq. (5). Note that the interpolation rule given by Eq. (6) is valid within any one element, whereas the integration region of Eq. (5) extends over a control volume that consists of several elements. Thus it is convenient to perform the integration indicated by Eq. (5) on an element-by-element basis and sum the results at a later time. Therefore we substitute Eq. (6) into Eq. (5) and perform the integration over a single element to arrive at the following expression:

$$\frac{\mathrm{d}}{\mathrm{d}t}\int_{S_e}\phi_i\sum_{j=1}^{3}(\phi_j w_j)\,\mathrm{d}A + \int_{S_e}\phi_i\left(\frac{\partial f}{\partial x}+\frac{\partial g}{\partial y}\right)\mathrm{d}A = 0 \tag{7}$$

The integration region S_e now is limited to a single element, and the weight functions ϕ_i are the linear interpolation polynomials associated with the three nodes of the element.

If the assumption is made that the fluxes vary linearly between nodes, then the second term in Eq. (7) can be integrated in closed form. This is an approximation since the expressions for f and g are nonlinear functions of the conserved quantities. The approach is consistent with finite volume formulations, however, and leads to a simple expression for the flux integral. An alternative is to integrate the expression numerically, an expensive procedure with a doubtful increase in quality of the overall solution. We therefore introduce the flux interpolation,

$$f(x, y, t) = \sum_{j=1}^{3}\phi_j(x, y)\, f_j(t) \tag{8a}$$

$$g(x, y, t) = \sum_{j=1}^{3}\phi_j(x, y)\, g_j(t) \tag{8b}$$

where the quantities f_j and g_j are the flux values at the node point j. Substitution into Eq. (7) gives

$$\frac{\mathrm{d}}{\mathrm{d}t}\int_{S_e}\phi_i\sum_{j=1}^{3}(\phi_j w_j)\,\mathrm{d}A + \int_{S_e}\phi_i\sum_{j=1}^{3}\left(\frac{\partial\phi_j}{\partial x}f_j+\frac{\partial\phi_j}{\partial y}\right)\mathrm{d}A = 0 \tag{9}$$

Evaluation of the above integrals over a triangular element is simplified by the use of area coordinates, a discussion of which may be found in any finite element text, see, for example, Cook.[13] The resulting integration reduces Eq. (9) to

$$\frac{\mathrm{d}}{\mathrm{d}t}\sum_{j=1}^{3}(m_{ij}w_j) + q_i = 0 \tag{10}$$

In the previous equation the element consistent mass matrix, m_{ij} is given by

$$m_{ij} = \frac{A}{12}\begin{bmatrix} 2 & 1 & 1 \\ 1 & 2 & 1 \\ 1 & 1 & 2 \end{bmatrix} \tag{11}$$

where A is the area of the element. The element flux vector q_i becomes

$$q_i = \frac{1}{6}[f_1(y_2 - y_3) + f_2(y_3 - y_1) + f_3(y_1 - y_2) - g_1(x_2 - x_3) - g_2(x_3 - x_1) - g_3(x_1 - x_2)] \tag{12}$$

where x_i and y_i are the Cartesian coordinates of the three node points that define the element. Note that the element flux vector q_i is independent of the node point i. This simplifies the implementation of the method since only one vector is calculated for each element.

Equations (10–12) represent the contribution of a single element to the Galerkin integral. The global discretized conservation equations are obtained by assembly of the element equations according to the Galerkin statement of Eq. (5) and proceeds in a manner identical to that commonly used in structural finite elements. The resulting set of global equations can be written as

$$\frac{d}{dt}\sum_{j=1}^{n}(M_{ij}w_j) + Q_i = 0 \tag{13}$$

where M_{ij} and Q_i are now the global consistent mass matrix and global flux vector, respectively. The sum extends over all nodes in the mesh.

B. Artificial Dissipation

A stable solution to Eq. (13) is not possible because the Galerkin discretization scheme is inherently underdissipative for hyperbolic problems.[14,15] Therefore we must add an artificial dissipation term which effectively damps numerical oscillations yet is conservative in that it adds no mass, momentum, or energy to the system. Here we follow the lead of Jameson and Baker,[2] Jameson et al.,[3] Jameson and Mavriplis,[4] and Mavriplis[5] in using an adaptive dissipation operator that consists of second and fourth differences of the flow variables. Thus the discretized form of Eq. (13) is written as

$$\frac{d}{dt}\sum_{j=1}^{n}(M_{ij}w_j) + Q_i - D_i = 0 \tag{14}$$

where the dissipation D_i is given by a sum over all the nodes that are connected to the central node i:

$$D_i = \sum_{k=1}^{m} d_{ik} \tag{15}$$

Here d_{ik} is given by

$$d_{ik} = R_{ik}[\epsilon_2(w_k - w_i) - \epsilon_4(\nabla^2 w_k - \nabla^2 w_i)] \tag{16}$$

and where $\nabla^2 w_i$ is an undivided Laplacian operator defined as

$$\nabla^2 w_i = \sum_{k=1}^{m}(w_k - w_i) \tag{17}$$

The adaptive coefficient ϵ_2 is defined as

$$\epsilon_2 = k_2 \max(\nu_{ik}, \nu_{kj}) \tag{18}$$

where ν_{ik} is a pressure sensitive term given by

$$\nu_{ik} = \frac{\left|\sum_{k=1}^{m}(p_k - p_i)\right|}{\sum_{k=1}^{m}(p_k + p_i)} \tag{19}$$

In the previous formulation given by Eqs. (15–19), the subscript k represents all of the nodes connected to node i and the subscript j represents all of the nodes connected to k. The second adaptive coefficient ϵ_4 is defined as

$$\epsilon_4 = \max(0, k_4 - \epsilon_2) \tag{20}$$

Finally, the dissipation scale factor R_{ik} is given by

$$R_{ik} = \frac{A_1 + A_2}{\Delta t_{ik}} \tag{21}$$

where A_1 and A_2 are the areas of the elements on either side of the line connecting nodes i and k, and Δt_{ik} is the signal propagation time from node i to k. The constants k_2 and k_4 are empirically determined through numerical experiments.

C. Boundary Conditions

The near field boundary condition consists of the requirement of flow tangency at the airfoil surface. It is implemented through the expression for the flux terms and is simply a statement that no flow should pass through an element edge that is adjacent to the airfoil. The actual values of velocity at the wall are not specified but are allowed to float freely and be updated at each time step. They naturally take on the tangency condition given the restriction on the fluxes.

Considering edge 1–2 of a triangular element to be coincident with the airfoil surface, we can rearrange Eq. (12) and set the average flux along this edge to zero. For flux terms that represent continuity or energy variables, the resulting boundary condition becomes

$$q_i = \frac{1}{6}[f_1(y_1 - y_3) + f_2(y_3 - y_2) + f_3(y_1 - y_2) - g_1(x_1 - x_3) - g_2(x_3 - x_2) - g_3(x_1 - x_2)] \tag{22}$$

Fluxes that represent momentum variables require an additional pressure term to be added to the previous equation. For the x-direction momentum equation, the additional term is given by

$$q_{x-\text{additional}} = \frac{1}{6}[(p_1 + p_2)(y_2 - y_1)] \tag{23a}$$

and in a similar fashion, we must add

$$q_{y-\text{additional}} = \frac{1}{6}[(p_1 + p_2)(x_1 - x_2)] \tag{23b}$$

to the y-direction momentum equation.

Far-field boundary conditions are somewhat more complicated because of the hyperbolic nature of the Euler equations and the fact that we are using a finite computational domain to simulate a physical problem that exists on an infinite plane. If flow conditions are specified at the outer edge of the region, a partially reflective boundary is created that echoes some of the energy in outgoing waves and eventually contaminates the solution. Instead, a nonreflective boundary condition is employed that allows outgoing waves to pass without reflection and does not generate extraneous information that can feed back into the computations. In this work the nonreflecting boundary conditions proposed by Hedstrom[16] and later used for two-dimensional unsteady flows by Venkatakrishnan and Jameson[8] are used. These boundary conditions are based on the incoming and outgoing characteristics of a system of one-dimensional hyperbolic partial differential equations and are employed in the direction normal to the far-field boundary.

Implementation of the far-field boundary conditions is accomplished by defining a set of fixed auxiliary node points and elements surrounding the outermost layer of the computational mesh. These points are not updated by the time-stepping procedure but are assigned values according to the nonre-

flecting boundary condition. Thus the boundary conditions are applied to the outer mesh nodes in an indirect sense through the flux terms in the last row of elements.

D. Grid Deformation

In this work a mesh deformation scheme is desired that efficiently moves grid points in a smooth fashion to conform with airfoil pitch or plunge motions. To be consistent with possible future work on three-dimensional aeroelastic configurations, points on the outermost boundary remain fixed whereas interior points are allowed to move. The movement of internal grid points is determined by first computing their displacements under the assumption that the mesh is attached to the airfoil as a rigid body. Next, each displacement is multiplied by a scale factor that depends on the original undeformed position of the grid point. Scale factors range from unity at the airfoil surface to zero at the outer boundary. These factors are computed only once at the start of the solution and vary linearly with distance from the airfoil. Thus the mesh movement scheme is very simple and requires only a few computations to determine new grid point coordinates after a given airfoil motion.

IV. Time-Stepping Procedure

The discretized form of the Euler equations with artificial dissipation terms, as given by Eq. (14), now takes the form of a system of ordinary differential equations, the solution of which can be obtained by a number of standard techniques. The method outlined here is to use an explicit five-stage Runge-Kutta procedure wherein the dissipation terms are evaluated only at the first two stages and frozen for the remaining three. A slight modification to the procedure is necessary, however, because the equations are not in explicit form due to the coupling present in the consistent mass matrix M_{ij}. Furthermore, as a result of the deforming mesh, M_{ij} is time dependent and cannot be removed from under the time derivative. To simplify the solution procedure, at the expense of true time accuracy, a diagonalized lumped mass matrix can be used. The other option is to perform an uncoupling operation on the consistent mass matrix during each time step. In the present work both options were used in an attempt to discover if time accuracy is adversely affected by the use of a lumped mass matrix.

A. Lumped Mass Matrix

A diagonalized lumped mass matrix can be obtained from the consistent mass matrix by summing all of the terms in a particular row and placing the result on the diagonal of that row.[17] With M_{ij} thus diagonalized, a Runge-Kutta time-stepping procedure is used to obtain the time history solution of the equations. For computational efficiency, the dissipative operator D_i is evaluated only during the first two stages. Using this simplification, the scheme is described as follows:

$$
\begin{aligned}
w_i^{(0)} &= w_i^n \\
w_i^{(1)} &= \frac{1}{M_{Lii}^{(1)}}\{M_{Lii}^{(0)} w_i^{(0)} - \alpha_1 \Delta t[Q_i^{(0)} - D_i^{(0)}]\} \\
w_i^{(2)} &= \frac{1}{M_{Lii}^{(2)}}\{M_{Lii}^{(0)} w_i^{(0)} - \alpha_2 \Delta t[Q_i^{(1)} - D_i^{(1)}]\} \\
w_i^{(3)} &= \frac{1}{M_{Lii}^{(3)}}\{M_{Lii}^{(0)} w_i^{(0)} - \alpha_3 \Delta t[Q_i^{(2)} - D_i^{(1)}]\} \\
w_i^{(4)} &= \frac{1}{M_{Lii}^{(4)}}\{M_{Lii}^{(0)} w_i^{(0)} - \alpha_4 \Delta t[Q_i^{(3)} - D_i^{(1)}]\} \\
w_i^{(5)} &= \frac{1}{M_{Lii}^{(5)}}\{M_{Lii}^{(0)} w_i^{(0)} - \alpha_5 \Delta t[Q_i^{(4)} - D_i^{(1)}]\} \\
w_i^{n+1} &= w_i^{(5)}
\end{aligned}
\tag{24}
$$

where M_{Lii} is the ith diagonal term from the lumped mass matrix, w_i is the vector of conserved quantities at node point i, and the coefficients α_i are given by

$$\alpha_1 = \frac{1}{4} \quad \alpha_2 = \frac{1}{6} \quad \alpha_3 = \frac{3}{8} \quad \alpha_4 = \frac{1}{2} \quad \alpha_5 = 1$$

Note, in Eq. (24), that the lumped mass matrix is updated during every stage of the Runge-Kutta scheme. This requires moving the mesh in five separate increments during a single time step. Thus a further simplification is proposed in which the lumped mass matrix is set to a single value for all stages of a time step. Here we choose to move the mesh to its position at the end of the time step, compute $M_{Lii}^{(5)}$, and use this value. Computations using both procedures will be performed to determine the differences between the two formulations.

B. Consistent Mass Matrix

In the case of a consistent mass matrix, the problem becomes more difficult because of the coupling due to the off-diagonal terms. We cannot simply divide through by the mass term as done in Eq. (24) but must explicitly solve for w_i after each stage of the Runge-Kutta scheme so that the flux and dissipation terms can be updated for the next stage. Fortunately M_{ij} is sparse so that a simple iteration procedure can be used to solve for the conserved quantities. Introducing the notation,

$$\tilde{w}_i = \sum_{j=1}^{n} (M_{ij} w_j) \tag{25}$$

the Runge-Kutta scheme becomes

$$
\begin{aligned}
\tilde{w}_i^{(0)} &= \tilde{w}_i^n \\
\tilde{w}_i^{(1)} &= \tilde{w}_i^{(0)} - \alpha_1 \Delta t[Q_i^{(0)} - D_i^{(0)}] \\
\tilde{w}_i^{(2)} &= \tilde{w}_i^{(0)} - \alpha_2 \Delta t[Q_i^{(1)} - D_i^{(1)}] \\
\tilde{w}_i^{(3)} &= \tilde{w}_i^{(0)} - \alpha_3 \Delta t[Q_i^{(2)} - D_i^{(1)}] \\
\tilde{w}_i^{(4)} &= \tilde{w}_i^{(0)} - \alpha_4 \Delta t[Q_i^{(3)} - D_i^{(1)}] \\
\tilde{w}_i^{(5)} &= \tilde{w}_i^{(0)} - \alpha_5 \Delta t[Q_i^{(4)} - D_i^{(1)}] \\
\tilde{w}_i^{n+1} &= \tilde{w}_i^{(5)}
\end{aligned}
\tag{26}
$$

After each stage of the previous scheme, we must solve for w_i to update the flux and dissipative operators. One option to accomplish this task is to invert the mass matrix and obtain w_i directly; however, this is an expensive operation and was not used here. Instead, a simple iteration procedure was implemented that produces good results and does not consume excessive computer resources. The procedure is summarized as follows. Let the result of any stage in the scheme of Eq. (26) be denoted by R_i. For example, after the first stage we have

$$R_i = \tilde{w}_i^{(1)}$$

Then the iteration procedure is

$$M_{Lii} w_{i(m+1)} = \sum_{j=1}^{n} (M_{Lij} - M_{ij}) w_{j(m)} + R_i \tag{27}$$

where M_{Lij} is the lumped mass matrix and M_{ij} is the consistent mass matrix. Since M_{Lij} is diagonal, the left-hand side of the previous equation represents a single term, making it easy to solve for w_i after each iteration. The scheme is started by choosing $w_{j(0)}$ as zero. Typically, five iterations were found to be necessary for w_i to approach within 5% of the fully converged value.

V. Results and Discussion

To demonstrate the validity and efficacy of the finite element formulation of the Euler equations, solutions were com-

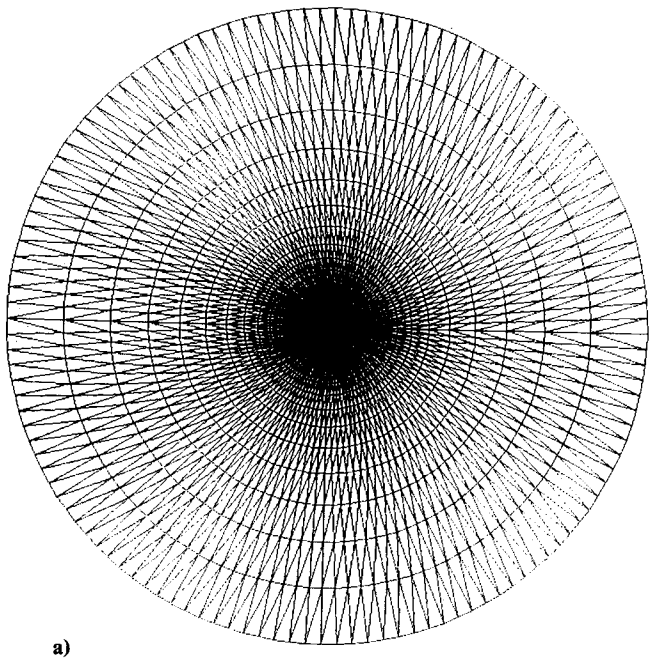

a)

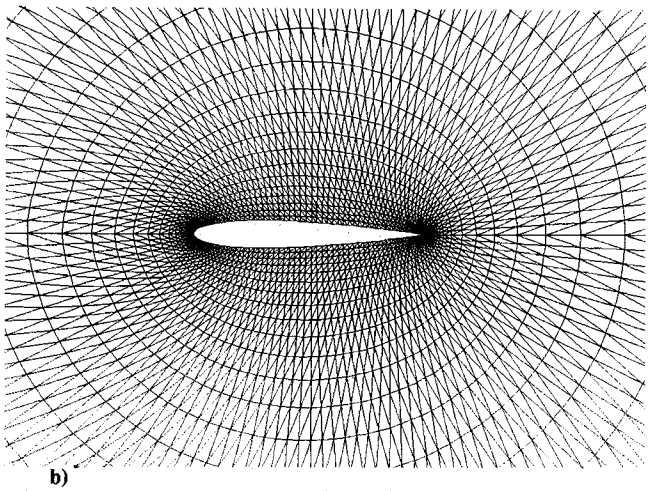

b)

Fig. 2 Undeformed grid about NACA 0012 airfoil: a) full field view and b) partial field view.

puted for both steady and unsteady transonic flows about a NACA 0012 airfoil. Computations were carried out using the unstructured grid shown in Fig. 2, which was derived from a structured quadrilateral cell O mesh. Although the grid of Fig. 2 appears to be structured, it is not. Unstructured regions exist near the airfoil leading and trailing edges, requiring the use of an unstructured solution routine. The same mesh is shown in Fig. 3 in the deformed state at a nose-up pitch angle of 15 deg. Note that the outermost nodes remain fixed in space, whereas the nodes on the airfoil surface move with the airfoil. The mesh consists of 4082 node points of which 124 are on the airfoil surface and 128 are on the far-field boundary, which is set at a radius of 25 chords.

A. Steady Solutions

Although the objective of the present work is to compute unsteady solutions to the Euler equations, the finite element concepts developed here were first tested on steady flow problems. The reason for this is that more high-quality published solutions exist for steady transonic flow than for unsteady flow. Solutions for a NACA 0012 airfoil in lifting and nonlifting supercritical flow are presented in the form of surface pressure coefficients in Figs. 4 and 5, respectively. In these figures we compare our finite element solutions with the results of Mavriplis,[18] obtained using advanced finite volume techniques. Note that in both figures, excellent agreement is shown between the two methods. In particular, the pressure jump across the shock is resolved in about the same number of nodes and the shock position is nearly identical for both solutions. It is clear from these figures that the finite element method produces a solution for steady transonic flows of a quality equal to that obtained using finite volume techniques.

B. Unsteady Solutions

In addition to the steady solutions mentioned earlier, the finite element method was used to compute the unsteady flowfield for the NACA 0012 airfoil oscillating in a sinusoidal fashion about the quarter-chord point. As a separate group, unsteady solutions for airfoil translation in the vertical direction were also computed. Again, the NACA 0012 airfoil was chosen for the computations because of the availability of finite volume solutions for comparative purposes.

The first case consisted of flow at Mach 0.8 with a peak oscillatory angle of attack of 5 deg, mean flow angle of zero, and a reduced frequency of $k = 1.0$. It is worth noting that this is a severe test of the solution scheme because of the large

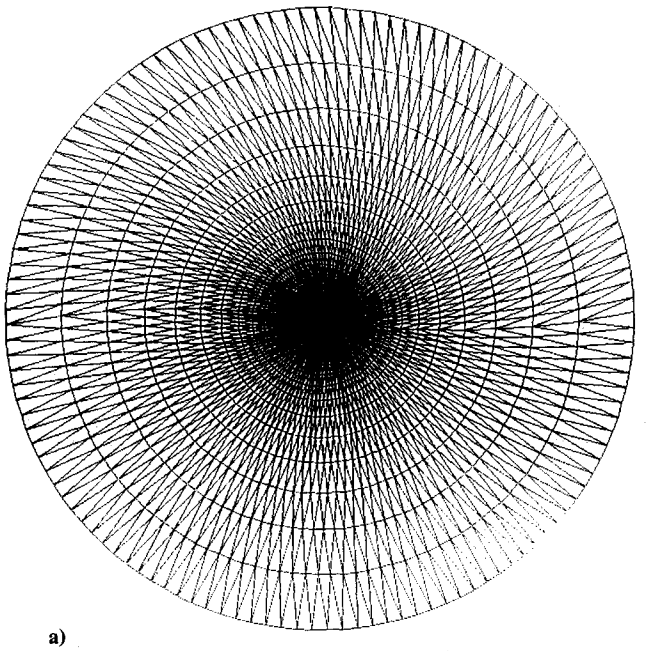

a)

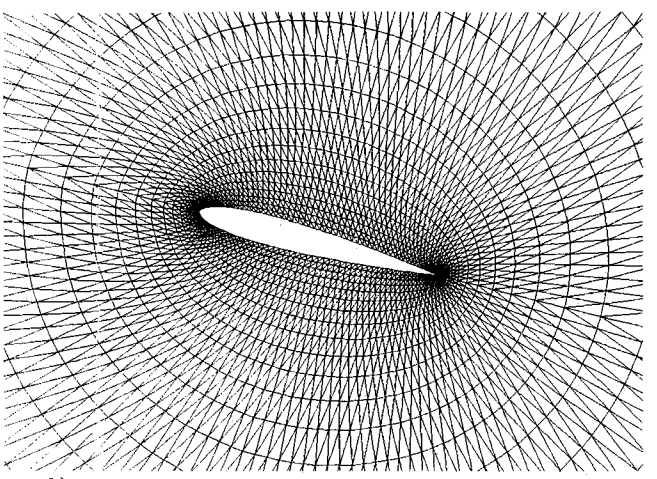

b)

Fig. 3 Deformed grid about NACA 0012 airfoil at nose-up pitch angle of 15 deg : a) full field view and b) partial field view.

amplitude of the motion and the high reduced frequency. Figures 6 and 7 present airfoil surface pressure coefficients computed at two different time points for this case using both the lumped and consistent mass formulations. A comparison with the finite volume results of Venkatakrishnan[19] is also presented in the same figure. From these figures we observe

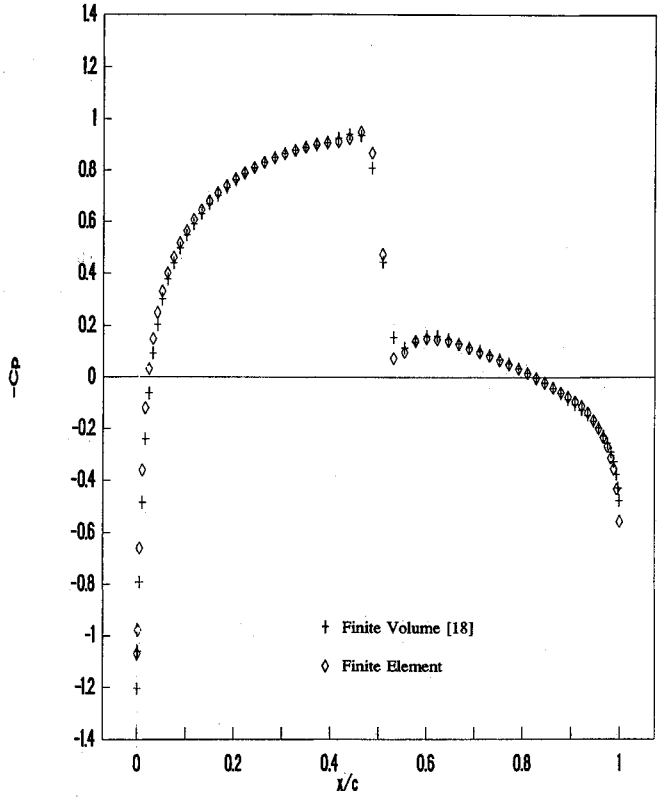

Fig. 4 Surface pressure coefficients for NACA 0012 airfoil in non-lifting flow at Mach 0.8, $\alpha = 0$ deg.

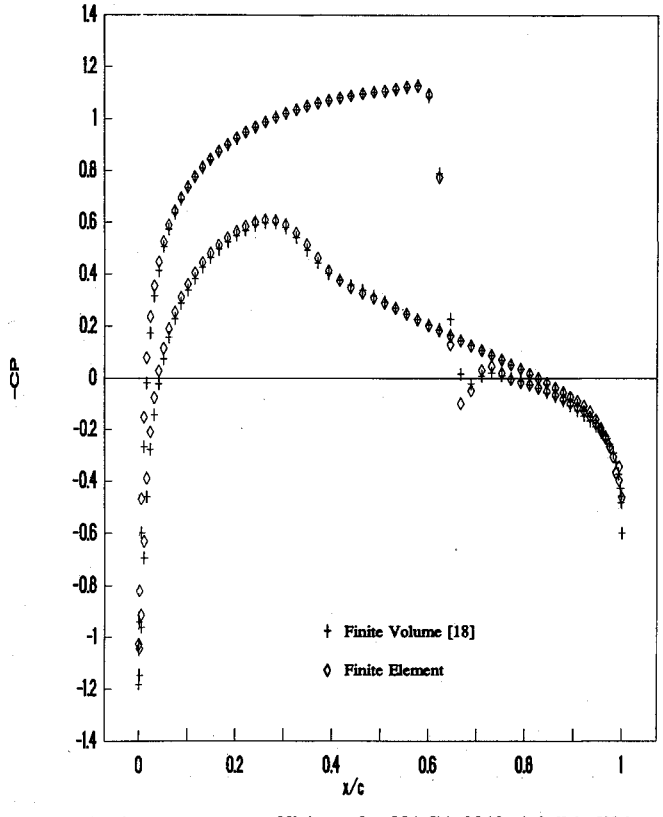

Fig. 5 Surface pressure coefficients for NACA 0012 airfoil in lifting flow at Mach 0.8, $\alpha = 1.25$ deg.

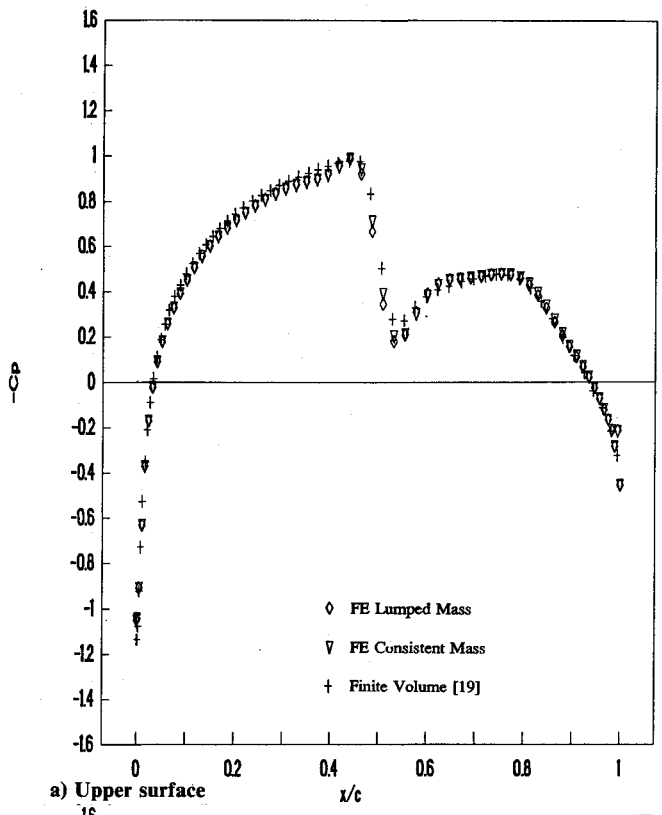

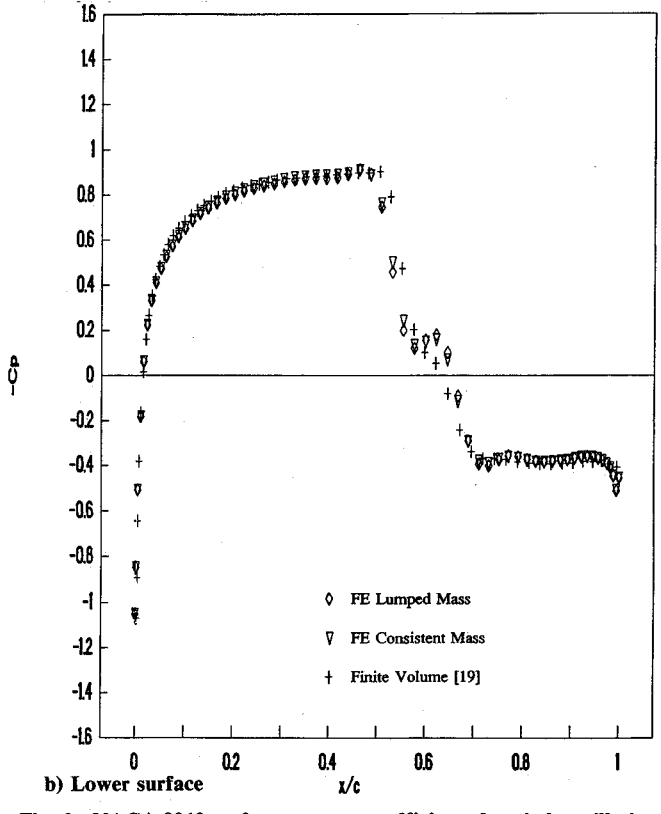

Fig. 6 NACA 0012 surface pressure coefficients for pitch oscillation about quarter-chord. Curves shown are taken at zero angle of attack during nose up pitching motion in the fourth cycle of oscillation, $M = 0.8$, $\alpha_m = 0.0$ deg, $\alpha_0 = 5.0$ deg, $k = 1.0$.

that excellent agreement exists between the finite volume and finite element methods. The shocks are well defined with little numerical overshoot and are positioned at the same location as predicted in the finite volume solution. The consistent mass formulation does not appear to provide an enhanced solution since there is a negligible difference between the two. This case was also run using the simplified procedure of updating the

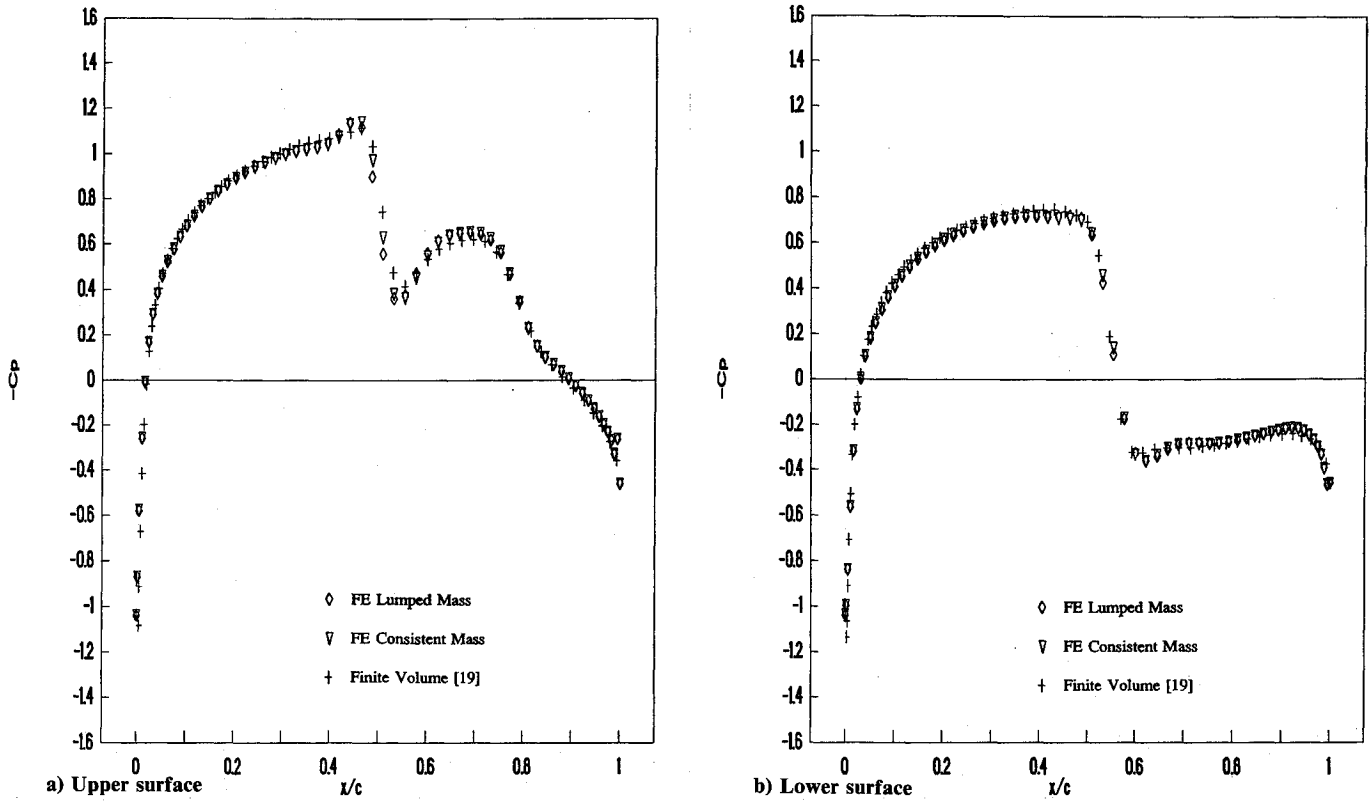

Fig. 7 NACA 0012 surface pressure coefficients for pitch oscillation about quarter-chord. Curves shown are taken at 433 deg angle of attack during nose up pitching motion in the fourth cycle of oscillation, $M = 0.8$, $\alpha_m = 0.0$ deg, $\alpha_0 = 5.0$ deg, $k = 1.0$.

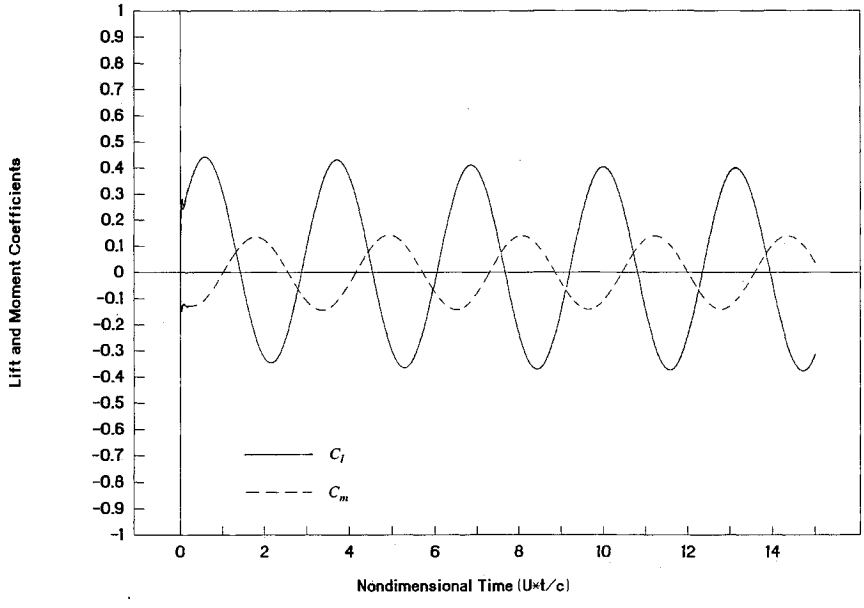

Fig. 8 Lift and moment coefficient time histories for lumped and consistent mass formulations showing indistinguishable differences between the two solutions, $M = 0.8$, $\alpha_m = 0.0$ deg, $\alpha_0 = 5.0$ deg, $k = 1.0$.

lumped mass matrix only once per time step. The solutions were nearly identical whether the updating was done once per time step or once per stage. Therefore we can conclude that stage update of the mass matrix is an unnecessary expense, at least for the small time step used here.

The insignificant difference between the lumped and consistent mass formulations is illustrated further by Fig. 8 that gives the airfoil lift and moment coefficients as a function of nondimensionalized time for both. The coefficients are so close as to be indistinguishable on the graph. The lift and moment coefficient results for the fourth oscillation cycle have been replotted in Fig. 9 to show a comparison with those of Ref. 19. Note the excellent agreement in both magnitude and phase shown in this figure.

The unsteady flowfield about an airfoil undergoing vertical translation was also investigated. The flow conditions chosen for this case were $M = 0.8$, peak vertical oscillation equal to 0.1 airfoil chords, mean flow angle of zero, and a reduced frequency of $k = 0.5$. Figures 10 and 11 show the resulting surface pressure coefficient plots at two different time points, as well as a comparison with an unpublished solution obtained by the authors using a cell centered finite volume method described in Ref. 11. Again, excellent agreement exists between the finite element and finite volume solutions. As with

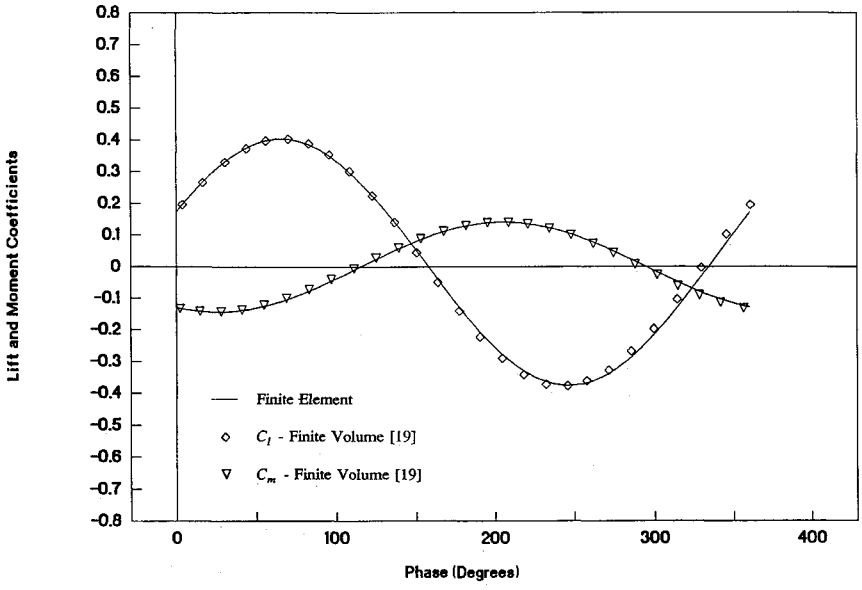

Fig. 9 Lift and moment coefficient versus phase relative to angle of attack during the fourth cycle of oscillation, $M = 0.8$, $\alpha_m = 0.0$ deg, $\alpha_0 = 5.0$ deg, $k = 1.0$.

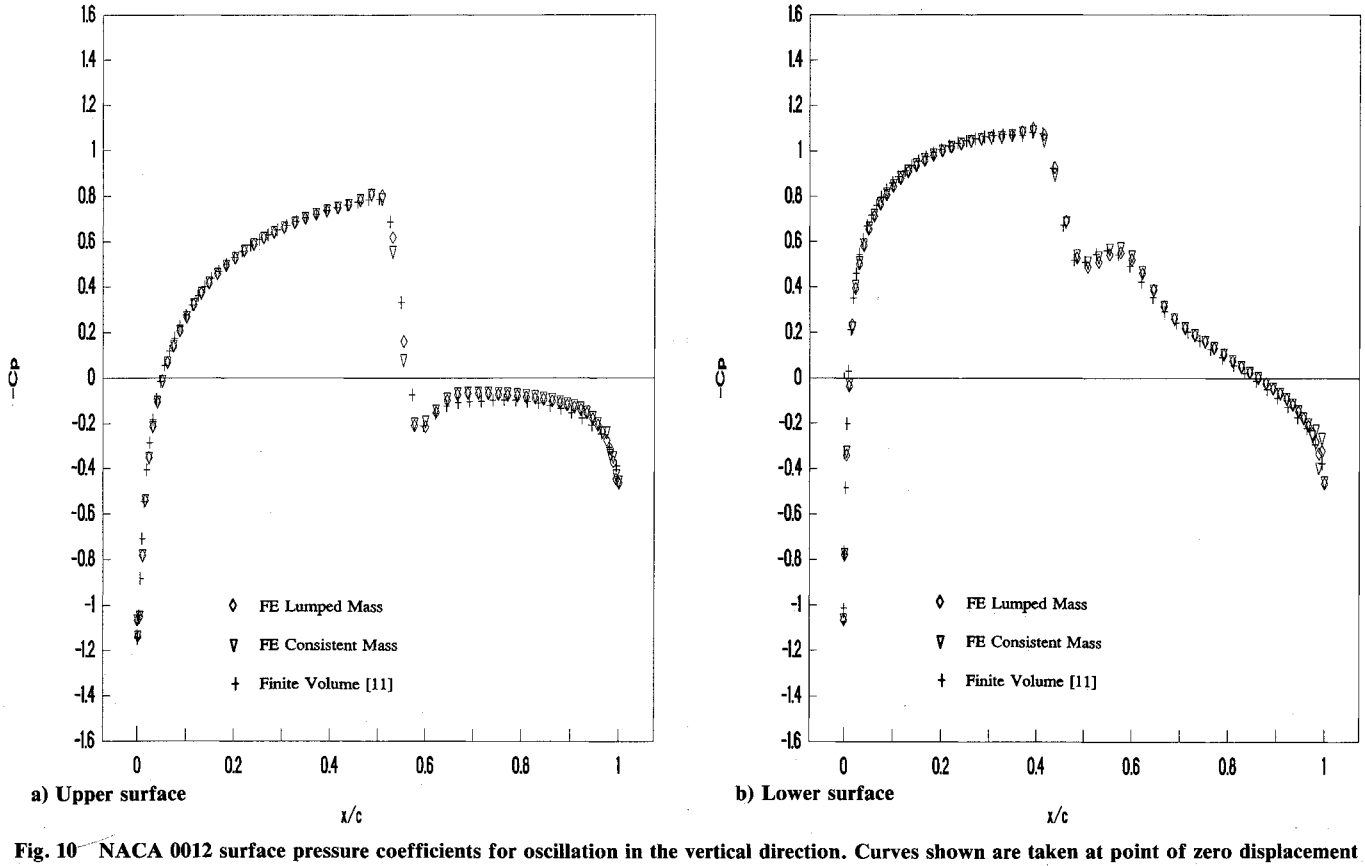

Fig. 10 NACA 0012 surface pressure coefficients for oscillation in the vertical direction. Curves shown are taken at point of zero displacement during upward motion of airfoil in the fourth cycle of oscillation; $M = 0.8$, $\alpha_m = 0.0$, $\alpha_0 = 0.0$ deg, $h_0 = 0.1$ chords, $k = 0.5$.

the pitching case, the consistent mass formulation does not provide a better quality solution. Both figures show only slight differences between the pressure coefficients calculated using the two methods.

Before dismissing the consistent mass formulation as unnecessary, it is important to point out that the cases shown here represent only a small fraction of possible configurations for unsteady flows. As can be seen in the figures, the grid used for the computations has extremely small elements in the leading- and trailing-edge regions. Since the allowable time step for the time-stepping procedure is dictated by the smallest element, the step size used in this analysis was very small. Typically 850 steps were necessary to compute one oscillation cycle for the $k = 1.0$ case. It is conceivable that, for larger element sizes, and in cases where the allowable Courant-Frederichs-Lewy (CFL) number is increased by the use of a technique such as residual averaging, or where an implicit time integration scheme is used, the consistent mass formulation may be necessary to insure true time accuracy. It was the intent of this paper to discuss the procedure for implementation of the consistent mass matrix and not to prove or disprove the need for its use.

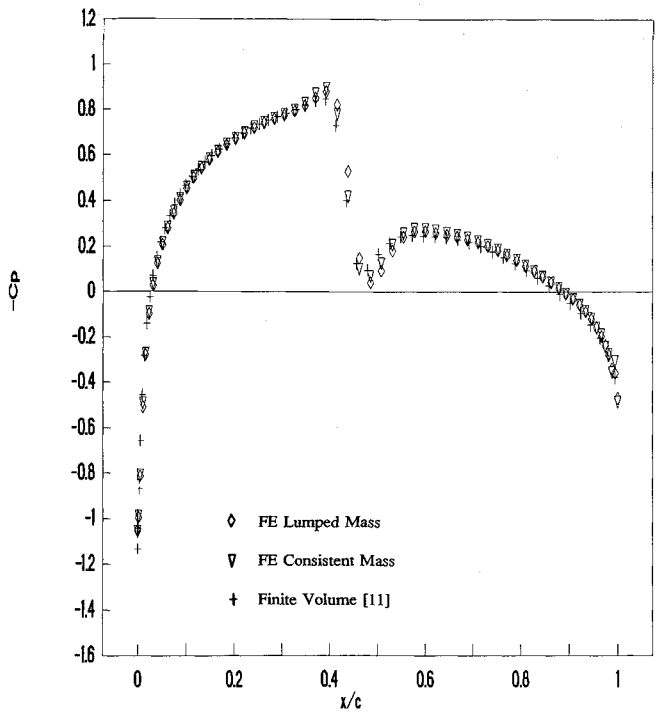

a) Upper surface

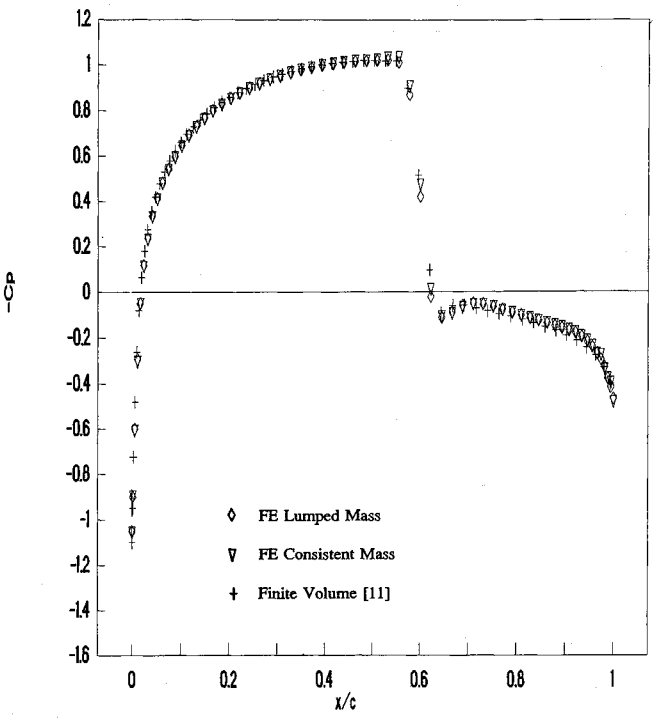

b) Lower surface

Fig. 11 NACA 0012 surface pressure coefficients for oscillation in the vertical direction. Curves shown are taken at point of maximum displacement during the fourth cyle of oscillation, $M = 0.8$, $\alpha_m = 0.0$ deg, $\alpha_0 = 0.0$ deg, $h_0 = 0.1$ chords, $k = 0.5$.

VI. Concluding Remarks

A finite element method was used to obtain unsteady flow solutions for an airfoil oscillating in pitch and plunge motion. Lumped mass and consistent mass formulations were used and comparisons were made with finite volume results. The main conclusions that can be drawn from this study are as follows:

1) The finite element method described in this paper provides an accurate solution for the steady and unsteady transonic flow about an isolated airfoil.

2) Unsteady flow computations performed using the finite element method have been shown, in comparisons with published and unpublished solutions, to provide a solution of a quality equal to advanced finite volume methods.

3) For the cases studied, the use of the consistent mass formulation did not provide an enhanced solution over the lumped mass approach. There may be other cases, however, where the use of a consistent mass matrix will improve the results. Of particular interest are problems with larger elements, when residual averaging methods are used to boost the allowable CFL number, or when an implicit integration scheme is used.

4) Updating of the lumped mass matrix once per time step gives results that are nearly identical to those obtained by updating once per stage of the Runge-Kutta scheme.

5) The use of the finite element formulation to model the fluid will aid in the eventual coupling of fluid and structural models during flutter calculations.

Acknowledgments

This research was supported by NASA Dryden Research Center Grant FDF NASA/A NCC 2- 374, with K. Gupta as grant monitor, and by NASA Lewis Research Center Contract NAS3-26064, with G. Stefko as contract monitor.

References

[1]Jameson, A., "Successes and Challenges in Computational Aerodynamics," AIAA Paper 87-1184, 1987.

[2]Jameson, A., and Baker, T. J., "Solution of the Euler Equations for Complex Configurations," *Proceedings of the AIAA 6th Computational Fluid Dynamics Conference* (Danvers, MA), AIAA, New York, 1983, pp. 293-302 (AIAA Paper 83-1929).

[3]Jameson, A., Schmidt, W., and Turkel, E., "Numerical Solutions of the Euler Equations by Finite Volume Methods Using Runge-Kutta Time Stepping Schemes," AIAA Paper 81-1259, June 1981.

[4]Jameson, A., and Mavriplis, D. J., "Finite Volume Solution of the Two-Dimensional Euler Equations on a Regular Triangular Mesh," AIAA Paper 85-0435, Jan. 1985.

[5]Mavriplis, D. J., "Accurate Multigrid Solution of the Euler Equations on Unstructured and Adaptive Meshes," *AIAA Journal,* Vol. 28, No. 2, 1990, pp. 213-221.

[6]Whitaker, D. L., and Grossman, B., "Two-Dimensional Euler Computations on a Triangular Mesh Using an Upwind, Finite Volume Scheme," AIAA Paper 89-0407, Jan. 1989.

[7]Edwards, J. W., and Thomas, J. L., "Computational Methods for Unsteady Transonic Flows," AIAA Paper 87-0107, Jan. 1987.

[8]Venkatakrishnan, V., and Jameson, A., "Computation of Unsteady Transonic Flows by the Solution of Euler Equations," *AIAA Journal,* Vol. 26, No. 8, 1988, pp. 974-981.

[9]Batina, J. T., "Unsteady Euler Airfoil Solutions Using Unstructured Dynamic Meshes," *AIAA Journal,* Vol. 28, No. 8, 1990, pp. 1381-1388.

[10]Batina, J. T., "Unsteady Euler Algorithm with Unstructured Dynamic Mesh for Complex-Aircraft Aerodynamic Analysis," *AIAA Journal,* Vol. 29, No. 3, 1991, pp. 327-333.

[11]Bendiksen, O. O., "A New Approach to Computational Aeroelasticity," AIAA Paper 91-0939, April 1991.

[12]Shames, J. H., and Dym, C. L., *Energy and Finite Element Methods in Structural Mechanics,* McGraw-Hill/Hemisphere, New York, 1985.

[13]Cook, R. D., *Concepts and Applications of Finite Element Analysis,* Wiley, New York, 1981.

[14]Donea, J., "Recent Advances in Computational Methods for Steady and Transient Transport Problems," *Nuclear Engineering and Design,* Vol. 80, July, 1984, pp. 141-162.

[15]Pulliam, T. H., "Artificial Dissipation Models for the Euler Equations," *AIAA Journal,* Vol. 24, No. 12, 1986, pp. 1931-1940.

[16]Hedstrom, G. W., "Nonreflecting Boundary Conditions for Nonlinear Hyperbolic Systems," *Journal of Computational Physics,* Vol. 30, Feb. 1979, pp. 222-237.

[17]Zienkiewicz, O. C., *The Finite Element Method,* McGraw-Hill, New York, 1977.

[18]Mavriplis, D. J., "Solution of the Two-Dimensional Euler Equations on Unstructured Triangular Meshes," Ph.D. Dissertation, Dept. of Mechanical and Aerospace Engineering, Princeton Univ., Princeton, NJ, Feb. 1987.

[19]Venkatakrishnan, V., "Computation of Unsteady Flows Over Moving Airfoils," Ph.D. Dissertation, Dept. of Mechanical and Aerospace Engineering, Princeton Univ., Princeton, NJ, Oct. 1986.